coatings

MDPI

Article

Hydrothermal Preparation of Calcium Aluminum Corrosion-Resistant Coatings on AZ91D Magnesium Alloy

Qingrong Tan [1], Ying Zhang [2,*], Min Jiang [1] and Jiyuan Zhu [1,*]

[1] Key Laboratory of Advanced Manufacturing and Automation Technology, Guilin University of Technology, Education Department of Guangxi Zhuang Autonomous Region, Guilin 541006, China; qingrongtanld@163.com (Q.T.); puppypriority@163.com (M.J.)
[2] Liuzhou Institute of Technology, Education Department of Guangxi Zhuang Autonomous Region, Liuzhou 545616, China
* Correspondence: feishmilying@163.com (Y.Z.); zhujiyuanscut@163.com (J.Z.)

Abstract: Magnesium alloys are widely used in all kinds of fields because of their excellent mechanical properties, but their application has been prevented by poor corrosion resistance. In this paper, $Mg(OH)_2$-$Ca(OH)_2$/$Al(OH)_3$/Al_2O_3 composite coatings with long-term corrosion resistance were fabricated on the surface of Mg alloys using the hydrothermal method. Among them, the calcium hydroxide/calcium nitrate–alumina coating successfully filled the cracks in the magnesium hydroxide coating. Meanwhile, we explored the influences of different heating times and temperatures on the coating and analyzed its composition. After immersing the coating in a 3.5% NaCl solution for 168 h, only a small portion of the surface dissolved. Electrochemical test results indicated that the corrosion potential and corrosion current density of the coating increased by three orders of magnitude, significantly improving corrosion resistance in comparison to bare samples. Adhesion tests showed that the coating exhibited good bonding performance to the substrate. This method features a simple, pollution-free preparation process and does not require complex instrumentation, thereby enhancing the longevity of the magnesium alloy.

Keywords: magnesium alloy; hydrothermal method; corrosion resistance; composite coating

check for updates

Academic Editor: Maria Vittoria Diamanti

Received: 20 May 2025
Revised: 10 June 2025
Accepted: 16 June 2025
Published: 17 June 2025

Citation: Tan, Q.; Zhang, Y.; Jiang, M.; Zhu, J. Hydrothermal Preparation of Calcium Aluminum Corrosion-Resistant Coatings on AZ91D Magnesium Alloy. *Coatings* **2025**, *15*, 722. https://doi.org/10.3390/coatings15060722

Copyright: © 2025 by the authors. Licensee MDPI, Basel, Switzerland. This article is an open access article distributed under the terms and conditions of the Creative Commons Attribution (CC BY) license (https://creativecommons.org/licenses/by/4.0/).

1. Introduction

Since magnesium was discovered, a significant amount of research has been performed on the properties of magnesium [1–3]. By using magnesium as a base material and incorporating various metallic and non-metallic elements [4–6], magnesium alloys exhibit unique characteristics such as impact resistance [7,8], electromagnetic shielding [9,10], efficient heat dissipation [11,12], and environmental friendliness [13–16]. Consequently, in the 21st century, magnesium alloys have found extensive use in multiple industries, particularly in the aerospace and automotive industries [17,18]. However, magnesium alloys corrode easily because of the low standard electrode potential of magnesium, and the oxides of magnesium alloys cannot effectively prevent corrosion [19–21]. This brings significant challenges for the practical utilization of Mg alloys [22]. Currently, the main approach is to apply coatings to the surface of Mg alloys to protect the substrate. Common methods include electrodeposition [23], micro-arc oxidation [24], anodizing [25], water-bath treatment [26], laser etching [27], and hydrothermal methods [28–30]. Compared to other techniques, the hydrothermal method has been extensively adopted due to its minimal equipment requirements and cost-effectiveness, being a simple procedure that does not generate hazardous pollutants and enables strong adhesion of the resulting coatings [31]. For

example, Zhang et al. [32,33]. used the hydrothermal method to prepare corrosion-resistant and friction-resistant coatings on magnesium-based surfaces, while Jia et al. employed the hydrothermal method to fabricate coatings on magnesium alloy surfaces, achieving an impedance as high as 10^9 $\Omega \cdot cm^2$ [34]. These studies proved the excellent performance of the hydrothermal method. In addition, the type of coating is also worth considering. Currently, chromium-based coatings are widely used. Although these coatings exhibit good corrosion resistance, the toxicity of chromium poses risks to the environment and human health [35]. Compounds of carbon and silicon elements, due to their environmental friendliness and biocompatibility, are reasonable to apply to magnesium alloy protection, where common coatings include calcium carbonate, calcium nitrate, and other types of coatings [36]. Studies such as those by Wang and Hou et al. [37,38] have demonstrated the preparation of calcium silicate and calcium carbonate coatings on the surface of a magnesium base, which protects the Mg substrate without causing pollution. However, these coatings may be prone to cracking and embrittlement, potentially leading to failure during long-term use. Based on this, considering the inherent strength and stability of aluminum and its oxides, the incorporation of related compounds enables improvements in both the corrosion resistance and mechanical strength of the composite coating. Meanwhile the dense properties of aluminum-based oxides can not only fill the cracks of carbonate/silicate coatings but can also improve the corrosion resistance of the coatings and prolong their service life [39].

In this study, a composite coating consisting of a magnesium hydroxide base layer and $Ca(OH)_2/Al(OH)_3/Al_2O_3$ protective layers is prepared on a Mg alloy surface using the hydrothermal method. The calcium–aluminum composite coating prepared by the hydrothermal method combines the excellent densification of calcium compounds with the superior strength of elemental aluminum oxides, which not only improves the densification and mechanical strength of the composite coating but also significantly enhances its corrosion resistance. Building upon the simplicity and environmental friendliness of the traditional hydrothermal method, this approach achieves an overall improvement in coating performance. The primary function of the $Ca(OH)_2/Al(OH)_3/Al_2O_3$ layer is to fill cracks in the $Mg(OH)_2$ coating, thereby enhancing the coating's corrosion resistance and mechanical strength. Adhesion tests demonstrate that the coating exhibits excellent bonding strength to the substrate. The entire preparation process generates no harmful by-products and requires neither extended processing time nor complex equipment. After immersion in a 3.5% NaCl solution for 168 h, the coating surface remains largely intact, with slight corrosion seen at the edges and corners. These results indicate the coating ensures substantial protection to the magnesium substrate, offering a reliable safeguard for the long-term application of magnesium alloys.

2. Materials and Methods

2.1. Materials

The AZ91D magnesium alloy was obtained from Dongguan Kuangyu Metal Materials Co., Ltd. (Dongguan, China), and the specimen surface area was 4 cm^2. Anhydrous ethanol and calcium oxide were obtained from Roen; aluminum nitrate nonahydrate and sodium hydroxide were purchased from Xilong (Foshan, China). The electric drying oven (101-1B) was purchased from Changge Mingtu Machinery Equipment Co., Ltd. (Changge, China). The magnetic stirrer was acquired from INTLLAB (Putrajaya, Malaysia), and the ultrasonic cleaner was purchased from Shenzhen Jiemeng Cleaning Equipment Co., Ltd. (Shenzhen, China). The image measuring system was purchased from Dongguan Yihui Optoelectronics Technology Co., Ltd. (Dongguan, China).

2.2. Preparation Process

Before the experiment, the magnesium alloy samples were polished with sandpaper of different grit sizes (600, 1000, 1500, and 2000 grit). The polished samples were cleaned in anhydrous ethanol for five minutes, washed with deionized water, and lastly air-dried. A total of 3 g of CaO $Al(NO_3)_3 \cdot 9H_2O$ and 0.3 g of NaOH were added to 30 mL of deionized water. The pH was maintained between 11 and 12, and the liquid was stirred at 30 r/min with a magnetic stirrer for 10 min to a colloidal state. The prepared suspension and the pretreated samples were placed in a 100 mL PTFE-lined autoclave and heated in an oven. The pressure inside the reactor was between approximately 0.47 MPa and 0.8 MPa. Based on the deposition characteristics of the first and second phases of magnesium alloy at different temperatures and times, the experiment was set with different temperatures (150–170 °C) and times (3 h–4 h) as control conditions. After the heating process, the samples were removed, washed with deionized water, and dried in an oven at 120 °C for 10 min. After heating, the samples were taken out, cleaned with deionized water, dried, and labeled LDH-53, LDH-63, LDH-64, LDH-73, and LDH-74. The fabrication procedure is depicted in Figure 1.

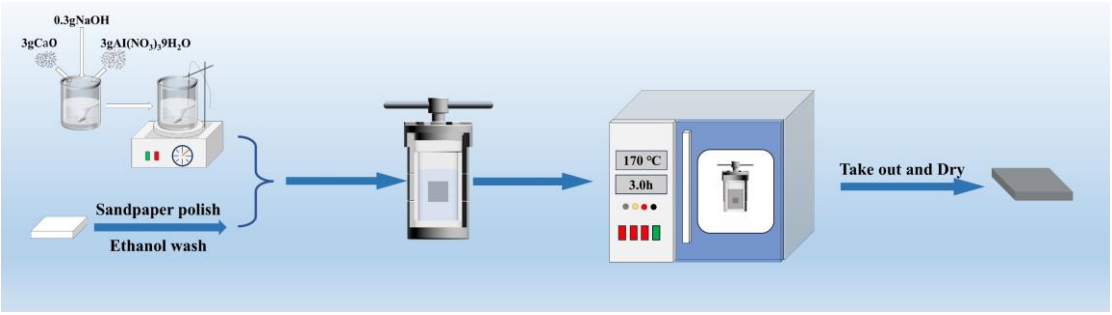


Figure 1. Coating fabrication process.

2.3. Characterize

The surface structural morphology of the composite coatings examined through scanning electron microscopy (SEM, TESCAN, Gemini SEM500, Oberkohen, Germany). The physical phase composition of the samples was investigated by X-ray diffraction (XRD, Bruker AXS, Karlsruhe, Germany) (test scanning angle: 2θ; range: 10–90°; target: CuKa target; test scanning speed: 6°/min; test wavelength: 1.54056A). The chemical composition and electron valence of the samples were measured and analyzed by X-ray photoelectron spectroscopy (XPS, Escalab 250Xi, Thermo Scientific, Waltham, MA, USA) (monochromatized Al Kα source; voltage: 1486.6 ev; 5 mA × 15 KV; test spot beam size: 700 × 300 μm; scan mode: CAE; fluence energy: 160 eV; narrow-spectrum scanning fluence energy: 40 eV; number of scans: 1).

2.4. Evaluation of Corrosion Performance

Electrochemical analysis of the coatings was performed with a CS2350H electrochemical workstation (Wuhan Corrtest Instruments Co., Ltd., Wuhan, China). The tests were performed at room temperature, with the workstation employing a standard three-electrode setup, in which platinum was the auxiliary electrode, and an Ag/AgCl electrode was used as the reference electrode. To maintain stability, the samples were tested at an open-circuit potential for 30 min prior to testing. Polarization plots were obtained at a scan rate of 1 mV/s. The potential was set from −0.5 to 1 V. The operating frequency range was from 0.01 Hz to 100,000 Hz with an AC amplitude of 5 mV.

2.5. Immersion Test

Immersion tests were used to evaluate the corrosion resistance of the coating. The tests were conducted at room temperature and atmospheric pressure following ASTM G31-72 standards [40]. Every 24 h, samples were taken out from the 3.5% NaCl solution, thoroughly rinsed with deionized water, and dried, and their mass reduction was measured with an electronic balance. Images were taken for surface assessment.

3. Results and Discussion

3.1. Surface Morphology

Figure 2 shows the surface morphology of the coating at various magnifications. In Figure 2, scratches left by polishing the magnesium alloy are visible in the flat regions, indicating a thin coating. The coating particles grow along these scratches, suggesting in situ formation of the coating. The raised parts consist of interlaced cubic crystals that combine into blocky aggregates, varying in size and growth direction. It can be observed that the polymer primarily comprises two microstructures: distinct hexagonal sheets and irregular polygonal sheets with uneven surfaces. Observing Figure 2a–c, cracks are found in the LDH-53 sample coating, and corrosion signs appear on the cubic sheets at higher magnifications. Likewise, Figure 2f,g show cracks in the LDH-63 sample coating, with corrosion appearing on the enlarged cubic crystals. But the coverage is better compared to LDH-53, with much smaller cracks, and crystalline growth is observed on the surface. In contrast, Figure 2i–k show that the LDH-73 sample coating has almost no cracks, with cubic sheets perfectly covering the cracked areas. The cubic flakes are larger in size and more numerous, and in the magnified image Figure 2k, no corrosion is observed on the cubic flakes. This indicates that the coating formed at 170 °C has the best coverage to effectively fill the cracks in the magnesium hydroxide. The thickness of the coating further demonstrates that coatings prepared at different temperatures have varying degrees of coverage; coatings at higher temperatures are thicker and provide better coverage on the substrate (Figure 2d,h,l).

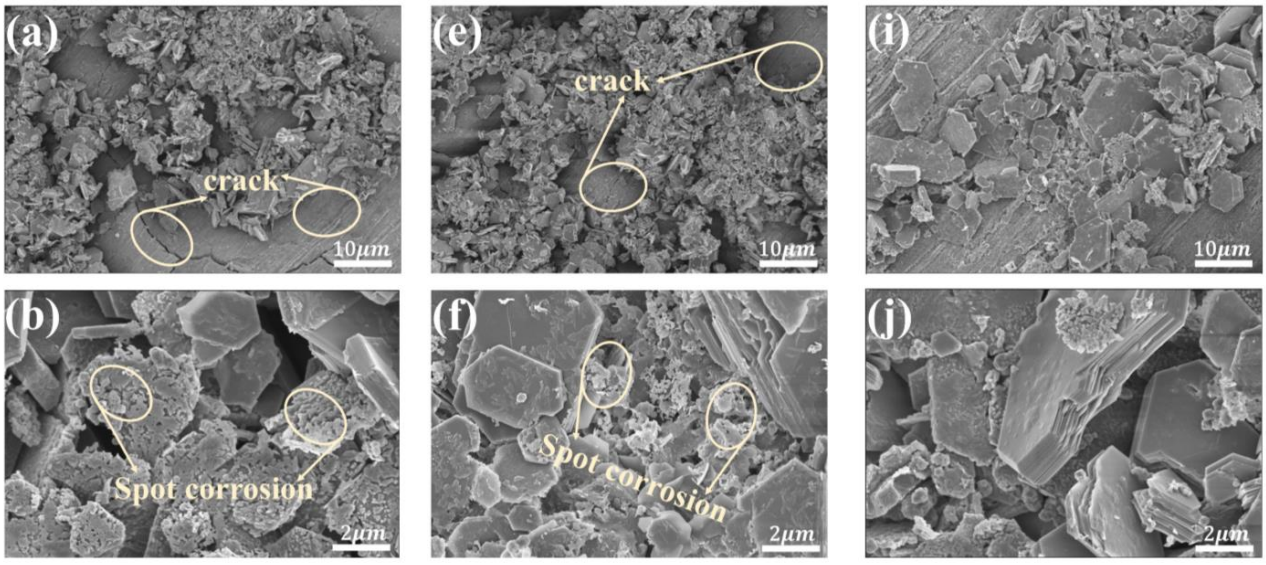


Figure 2. *Cont.*

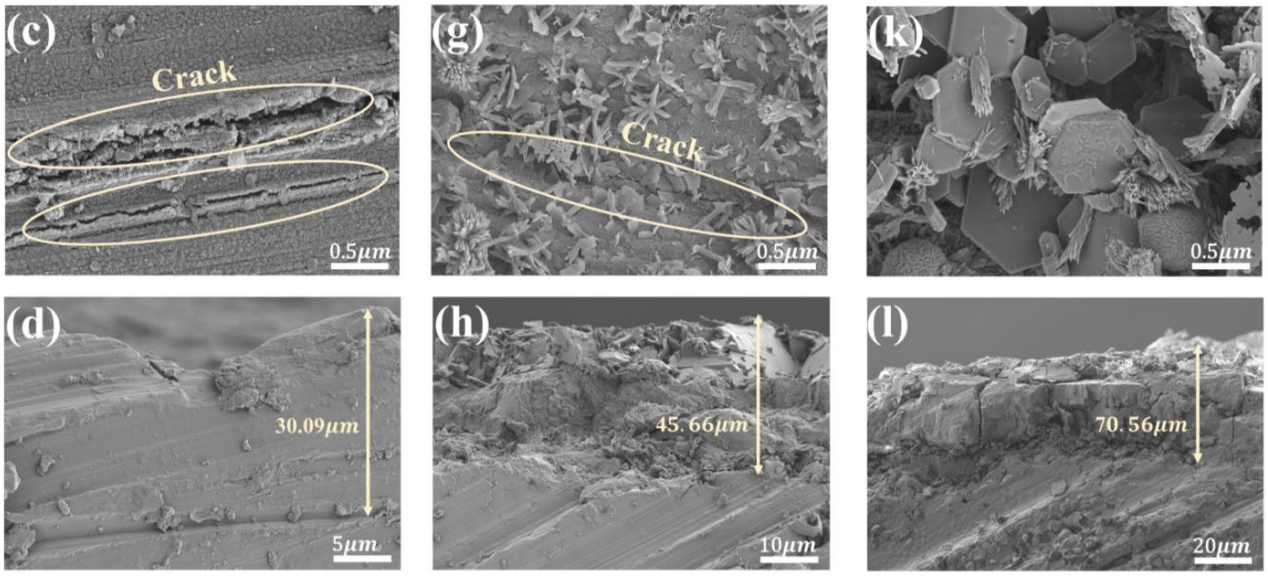


Figure 2. SEM images of the coatings: (**a**–**d**) LDH-53; (**e**–**h**) LDH-63; and (**i**–**l**) LDH-73.

3.2. Surface Composition Analysis

To better distinguish the surface composition of the coating, XRD was employed to identify the phase, and the XRD results of the LDH-73 sample were selected to represent the coating. Figure 3b shows the XRD pattern of the Mg substrate, with characteristic peaks at 34.47° (002), 36.69° (101), 47.926° (102), 57.516° (110), 63.21° (103), 67.49° (200), 70.19° (201), and 72.69° (004), corresponding to Mg (PDF#01-079-6692). Peaks at 36.11° (411), 38.13° (420), 40.07° (332), 41.94° (422), 62.20° (550), 63.58° (640), and 64.94° (721) correspond to Mg17Al12 (PDF#04-014-7592). Figure 3c displays the XRD pattern of the LDH-73 sample. The characteristic peaks at 18.58° (001), 32.82° (100), 37.98° (011), and 50.51° (012) in the XRD pattern correspond to the $Mg(OH)_2$ (PDF#04-011-5938) crystal. The characteristic peaks at 28.72° (100), 18.10° (001), 34.16° (011), and 64.36° (012) correspond to the $Ca(OH)_2$ (PDF#97-001-5471) crystal. The peaks at 38.01° (002) and 63.8° (300) correspond to the $Al(OH)_3$ (PDF#97-016-4050) crystal, while the peaks at 38.70° (110) and 59° (116) correspond to the Al_2O_3 (PDF#97-000-9770) crystal.

$Mg(OH)_2$ and $Ca(OH)_2$ are formed under alkaline conditions, $Al(OH)_3$ is hydrolyzed from aluminum nitrate nonahydrate, and Al_2O_3 is generated by the breakdown of $Al(OH)_3$ at high temperature and pressure. These diffraction peaks exhibit high intensity and sharp profiles, indicating a large grain size, high content, good crystallinity, and broader coverage of the Mg substrate, which tremendously hamper corrosion process.

To analyze the chemical states and makeup of the sample surface, XPS testing was conducted. Figure 3a shows the survey XPS spectrum of the coating, revealing the existence of C, N, O, Mg, Al, and Ca. Figure 3d–i display the C1s, O1s, Al2p, N1s, Mg1s, and Ca2p spectra, respectively. The detailed C1s spectrum displays binding energies at 284 eV, 286 eV, and 289 eV related to C–C, C–O–C, and O–C=O bonds. The N1s spectrum displays binding energies at 399.6 eV, 403.0 eV, and 406.8 eV related to metal nitrates, $NSiO_2$, and nitrates, respectively. The O1s spectrum shows binding energies at 529.5 eV, 531.3 eV, and 532.6 eV linked to Al_2O_3, metal hydroxides, and silicates, respectively. The Mg1s spectrum presents binding energies at 1303.3 eV and 1304.5 eV related to metallic Mg and $Mg(OH)_2$, respectively. The Al2p spectrum indicates a binding energy at 74.1 eV related to Al_2O_3. The Ca2p spectrum displays binding energies at 346.8 eV and 350.7 eV linked to the Ca 2p3/2 and Ca 2p1/2 electronic states, indicating that the main component is $Ca(OH)_2$. The presence of N1s can come from the atmosphere. XPS and XRD analyses indicate that the sample surface consists of $Mg(OH)_2$, $Al(OH)_3$, Al_2O_3, and $Ca(OH)_2$. The main component of the coating is magnesium

hydroxide, which, as a corrosion product of magnesium alloy, acts as a protective oxide film on the surface and effectively slows down corrosion. Aluminum hydroxide possesses covalent bonding characteristics and corrosion resistance, effectively resisting electrolyte ions and neutralizing acidic corrosive media, thereby reducing the corrosion rate. Calcium hydroxide originates from the hydrolysis of calcium oxide in alkaline solution; it is strongly alkaline, readily absorbs carbon dioxide and moisture from air, and neutralizes acidic substances in the environment, reducing corrosion on the Mg alloy surface. In addition, EDS scans were conducted on the coatings. For the LDH-53 (Figure 4a–c) and LDH-63 coating (Figure 4f–j) samples, the surface is primarily composed of magnesium and oxygen, which is related to the poor coverage on the magnesium substrate. The low content of calcium and aluminum elements indicates that the hydroxides of calcium and aluminum are less abundant, leading to poor coverage. In contrast, for the LDH-73 coating sample (Figure 4k–o), the surface elements are mainly oxygen and calcium. Based on the ratio of O to Ca (55.83:29.69 = 1:2), it can be inferred that the coating is calcium hydroxide. This suggests that the coating provides better coverage on the substrate with a higher content.

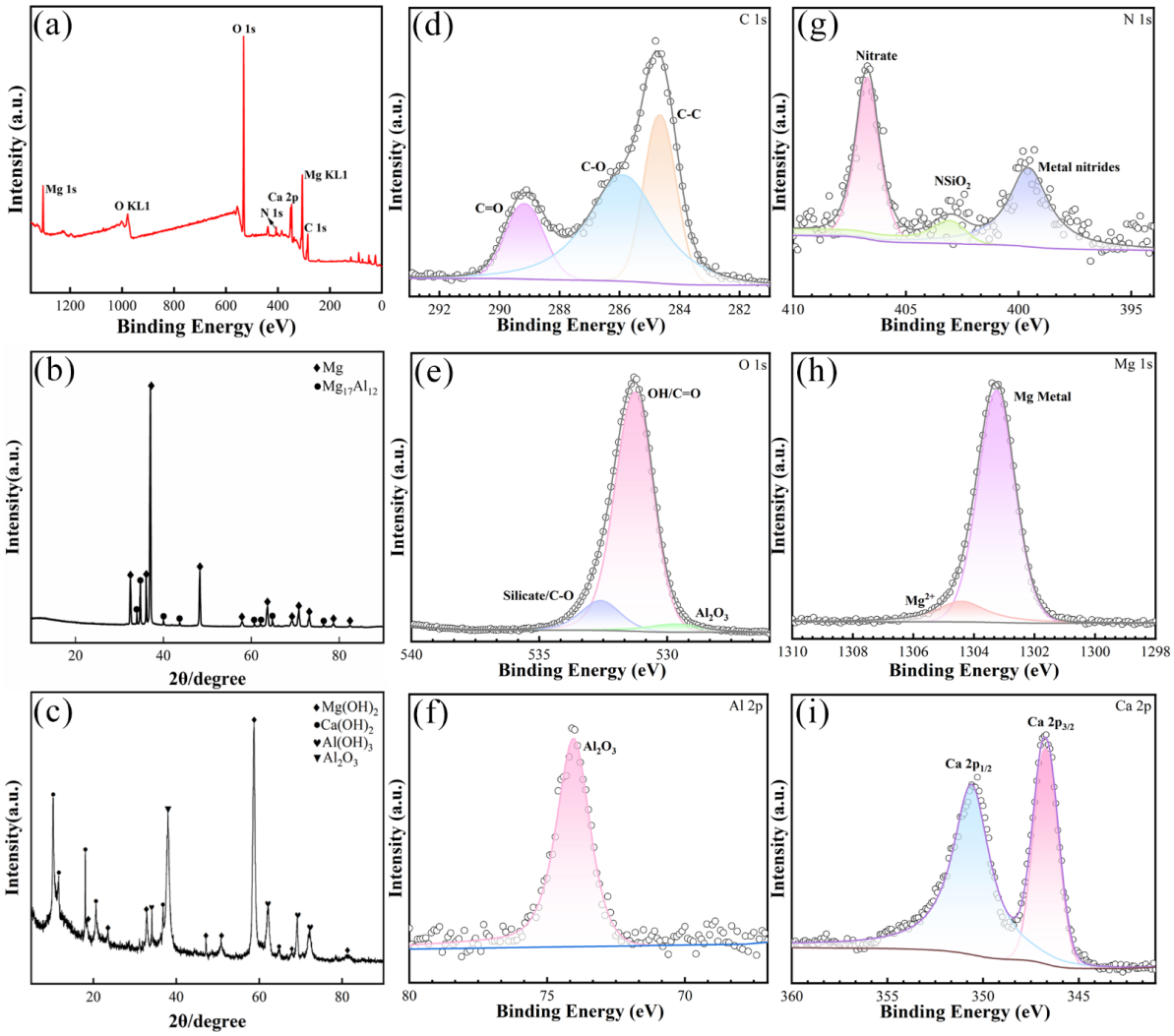


Figure 3. XPS scanning spectrum of LDH-73 (**a**); X- ray diffraction pattern of AZ91D alloy (**b**); X-ray diffraction pattern of coating (**c**); LDH-73 sample narrow scanning spectrum: (**d**) C 1s; (**e**) O 1s; (**f**) Al 2p; (**g**) N 1s; (**h**) Mg 1s; and (**i**) Ca 2p.

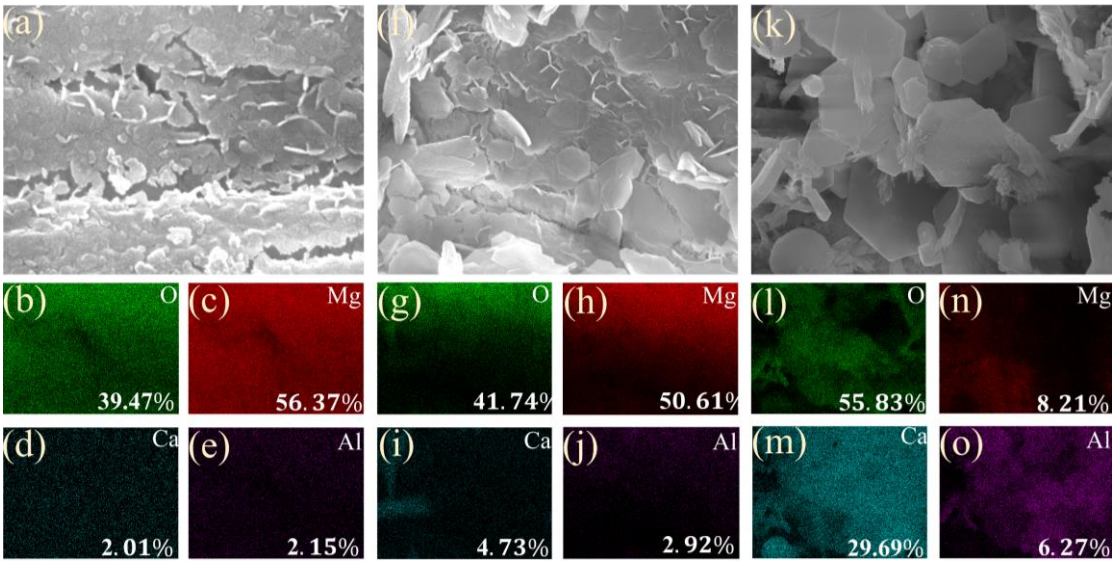


Figure 4. EDS spectral scanning: LDH-53 (**a**–**e**); LDH-63 (**f**–**j**); and LDH-73 (**k**–**o**).

3.3. Coating Formation Mechanism

According to the XRD and XPS data, the coating primarily comprises $Mg(OH)_2$, $Al(OH)_3$, Al_2O_3, and $Ca(OH)_2$. This is related to the reaction solution. When sodium hydroxide is added to deionized water to create an alkaline environment, the pH of the solution increases significantly, reaching approximately 11. After the addition of calcium oxide, it reacts with water, and the formation of calcium hydroxide ($Ca(OH)_2$) spontaneously dissolves, causing the pH to rise further. Finally, aluminum nitrate nonahydrate ($Al(NO_3)_3 \cdot 9H_2O$) is added, at which point aluminum ions (Al^{3+}) begin to release and react with calcium hydroxide, forming aluminum hydroxide or other aluminum-based compounds. The pH of the solution then stabilizes, reaching 12.

When the magnesium alloy is placed in a hydrothermal autoclave, it is subjected to high temperature and pressure. In an alkaline environment, magnesium ions are first produced, leading to the formation of abundant magnesium hydroxide precipitates. Meanwhile, calcium and aluminum ions in the solution react with hydroxide ions to produce calcium hydroxide and aluminum hydroxide precipitates. Under high temperature and pressure, aluminum hydroxide decomposes into α-alumina [41], which adheres to the aluminum hydroxide coating surface. The following is the reaction process:

$$Mg \rightarrow Mg^{2+} + 2e^-$$
$$Mg^{2+} + 2OH^- \rightarrow Mg(OH)_2 \downarrow$$
$$Al^{3+} + 3OH^- \rightarrow Al(OH)_3 \downarrow$$
$$Al(OH)_3 + OH^- \rightarrow Al(OH)_4^-$$
$$2Al(OH)_4^- \rightarrow \alpha - Al_2O_3 \downarrow$$

3.4. Corrosion Behavior

To compare the corrosion resistance of coatings fabricated in different conditions, electrochemical tests were conducted on all samples. Figure 5a–c show the Nyquist, Bode, and phase angle plots of the Mg substrate and coated samples (LDH-53, LDH-63, LDH-64, LDH-73, and LDH-74) immersed in 3.5% sodium chloride solution. Figure 5a shows that the capacitive arcs of all hydrothermally prepared coatings are obviously larger than the bare substrate, indicating superior corrosion resistance. A larger capacitive arc radius corresponds to higher charge transfer resistance and lower electron exchange rates [42]. For metals, lower electron exchange rates are related to low corrosion rates and excellent

corrosion resistance. The polarization curves in Figure 5b and the phase angle plots in Figure 5c also demonstrate the good corrosion resistance of the coatings. The current density of the magnesium substrate is 3.2973 × 10^{-5} A/cm^2, while all coated samples exhibit higher current densities than the substrate. According to electrochemical theory, materials with high corrosion resistance exhibit lower positive corrosion potentials and current densities [43]. The Bode plot in Figure 5c further confirms the corrosion resistance of the coatings. Generally, higher |Z| values in the Bode plot correspond to better corrosion performance. As shown in Figure 5c, the magnesium substrate displays a |Z| value of approximately 1.1 × 10^3, while all treated samples exhibit larger |Z| values than the Mg substrate. Among them, the LDH-73 coating presents the highest |Z| value, indicating its superior corrosion resistance. Figure 5d,e show the equivalent circuits of the magnesium substrate and LDH-73 coating, respectively. R_s represents solution resistance, R_f coating resistance, R_{ct} transfer resistance, R_L inductive resistance, and L inductance; L mainly arises from corrosion of the Mg substrate by the corrosive solution [44]. Compared with the Mg alloy substrate, the inductive loop is absent in the LDH-73 coating, indicating that substrate corrosion has been prevented [45]. A constant phase element (CPE) was employed instead of an ideal capacitor. The R_{ct} value is a key parameter for evaluating coating corrosion resistance [46]. Equivalent circuit fitting results show that the R_{ct} value of LDH-73 is much higher than that of AZ91D; results are shown in Table 1. Corrosion potential and corrosion current density were obtained by Tafel extrapolation from the polarization curves [47]; results are presented in Table 2. Figure 6 shows the error bar chart for the corrosion current density and voltage of the coating. It can be observed that the corrosion current density of the Mg substrate is the highest, while the coating exhibits a more positive corrosion voltage. This indicates that the coating has significantly better corrosion resistance compared to the magnesium substrate. Additionally, when compared with other coating preparation methods, it can be seen that the hydrothermally prepared coating demonstrates the best performance. Not only does it have the greatest thickness, but it also exhibits the strongest corrosion resistance Table 3.

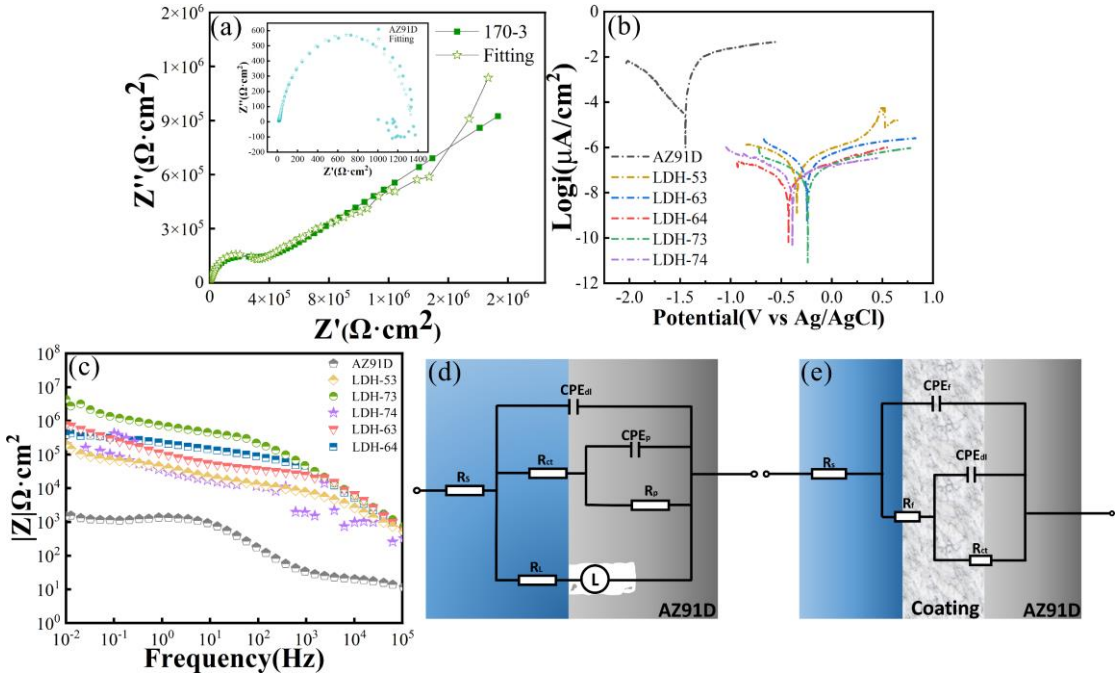


Figure 5. Different samples in 3.5 wt% NaCl solution: (**a**) potentiodynamic polarization curves (**b**) Nyquist plot; (**c**) bode plot of |Z| versus frequency; and (**d**) the equivalent circuit model of AZ91D magnesium alloy and LDH-73 sample (**e**).

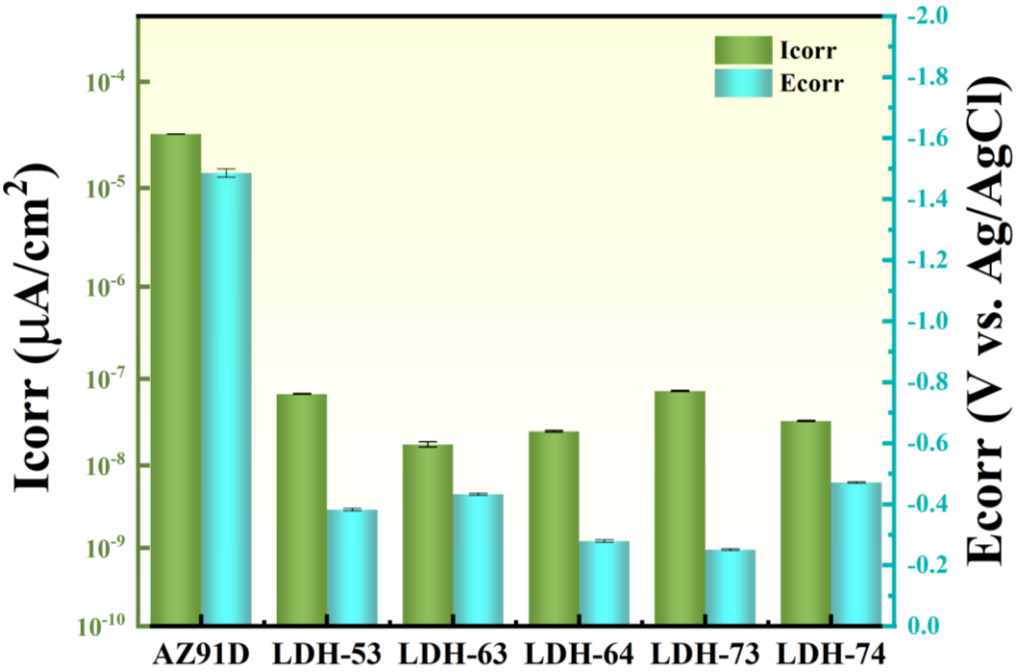


Figure 6. Error bar chart for current density and voltage.

Table 1. Fitting results of the EIS data.

Sample	R_S (Ω cm^2)	R_f (Ω cm^2)	CPE_{dl} (μFcm^{-2}·s$^{(a-1)}$)	R_{ct} (Ω cm^2)
Substrate	6.35	-	45	765
LDH-73	188.8	2.1835×10^5	0.89445	3.0782×10^6

Table 2. Electrochemical data of the coatings and substrate.

Coatings	Icorr (μA/cm^2)	Ecorr (V vs. Ag/AgCl)	η (%)
LDH-53	6.7599×10^{-8}	−0.38819	0.0015634
LDH-63	1.856×10^{-8}	−0.43459	0.00039361
LDH-64	2.4895×10^{-8}	−0.28181	0.00052798
LDH-73	7.3719×10^{-8}	−0.25245	0.0014364
LDH-74	3.3724×10^{-8}	−0.47287	0.00071521
Substrate	3.2973×10^{-5}	−1.4924	0.69929

Table 3. Comparison of different treatment methods.

Method	Corrosion Current Density (μA/cm^2)	Coating Thickness (μm)
Hydrothermal Method	0.0000007	30–70
Anodization	0.008	8–12
Electrophoretic Deposition	0.002	12–18
Micro-Arc Oxidation	0.003	24–40

3.5. Immersion Test

Immersion testing was employed to assess the long-term corrosion resistance of coatings. The LDH-73 coating sample and magnesium substrate sample were soaked in 3.5% NaCl solution for 168 h, with samples taken out every 24 h for rinsing, drying, and weighing. Figure 7a displays the surface characteristics of the magnesium substrate and LDH-73 coated samples after 24 h. Over time, cracks begin to appear on the magnesium substrate surface, which grow larger with time. After 168 h, more extensive spalling and pitting occur on the substrate. Observations of the coated samples reveal a small notch at the lower left corner after 72 h immersion, which enlarges over time, along with a

small notch forming at the upper right corner. These effects are attributed to chloride-induced corrosion.

Figure 7b shows weight loss data recorded every 24 h. The magnesium substrate experiences significant mass loss after 24 h, indicating rapid corrosion. The LDH-73 coated samples exhibit lower mass loss and slower reduction rates, demonstrating excellent corrosion resistance and the ability to resist penetration by corrosive agents.

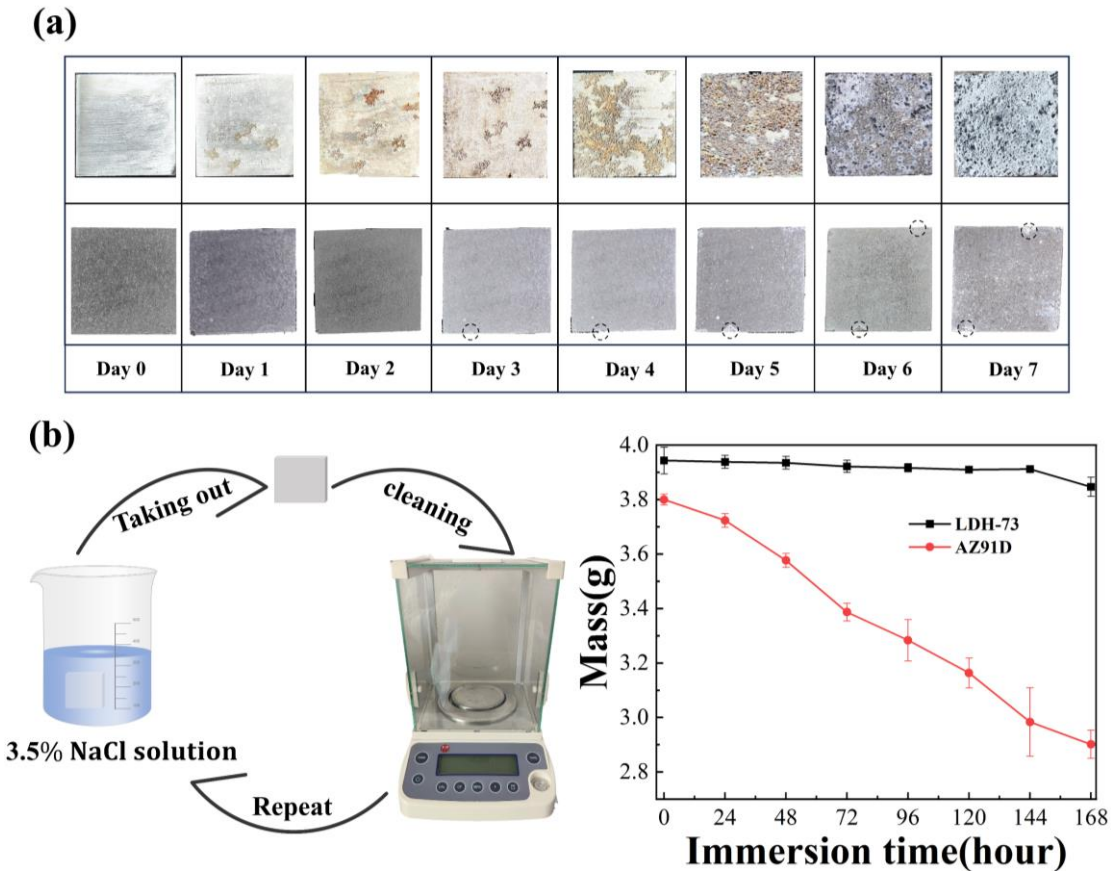


Figure 7. (**a**) The images of Mg substrate and LDH-73 coatings in 3.5 wt% NaCl solution. (**b**) Immersion test data of Mg substrate and LDH-73 coatings in 3.5 wt% NaCl solution.

3.6. Adhesion Properties

Adhesion is an important indicator for evaluating corrosion resistance and coating durability. Good adhesion to the substrate can block the fall of the coating. Therefore, an adhesion cross-cut tape test was conducted to assess the coating's adhesion, and Figure 8 shows the test procedure. According to ASTM-D3359 [48], a blade was used to score longitudinal and transverse lines on the coating surface, creating a grid. Small flakes appeared at the intersections. Loose flakes were brushed off. Then adhesive tape was firmly applied over the scored area and peeled off at a 180° angle. Microscopic observation showed that the cut edges of the coated sample were mostly smooth, with no obvious peeling. The percentage of the coating retained, calculated after microscope observation, is approximately 95%. Adhesion was evaluated according to ISO 2409-2020 [49], achieving the highest grade of 5B. The results indicate that the coating adhered to the substrate well.

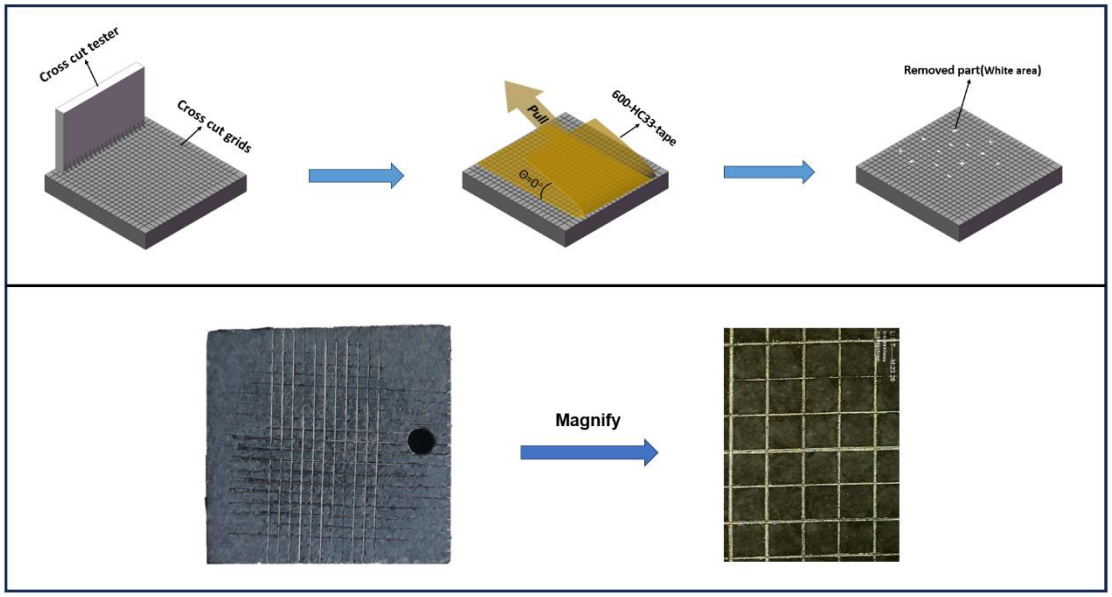


Figure 8. Cross-cut tape test on the coatings.

3.7. Corrosion Behavior Mechanisms

Figure 9 demonstrates the corrosion behavior of the magnesium substrate and LDH-73 coated in 3.5% NaCl solution. Initially, the unprotected Mg substrate was directly exposed to the corrosive solution, where chloride and hydroxide ions eroded the magnesium alloy surface, forming dispersed magnesium hydroxide and magnesium chloride. As corrosion progressed, these initial layers failed to protect the underlying substrate [50], leading to deeper corrosion and plotting, causing severe damage to the magnesium substrate.

In contrast, the LDH-73 coated samples were protected by the coating, hampering the ingress of external corrosive mediums. The coating is dominated by magnesium hydroxide, with aluminum hydroxide, calcium hydroxide, and alumina serving auxiliary roles. Since the coating was fabricated via the hydrothermal method, the resulting $Mg(OH)_2$ layer is thicker and denser than naturally formed coatings, with improved continuity [51]. Calcium hydroxide, aluminum hydroxide, and alumina fill and bond cracks in the magnesium hydroxide layer, strengthening the protective film. The immersion test confirmed this process, which correlates with the sharpness and peak intensity of the XRD pattern, demonstrating that the coating surface has good crystallinity, a more ordered structure, and fewer defects. This contributes to the formation of a dense and stable protective layer, enhancing its protective performance. The alumina component, due to its high hardness and density, enhances the coating's strength, while the hydroxides exhibit good crystallinity, effectively delaying electrolyte penetration to the magnesium substrate, thus providing corrosion protection. Such composite coatings effectively isolate the magnesium substrate from corrosive ions in solution, greatly slowing the corrosion process. Nevertheless, over time, corrosion signs appeared at stress concentration sites in the coating, where geometric constraints hindered proper coating growth, reducing resistance to corrosive ion penetration. Once coating defects form, corrosion of the coating progressively worsens.

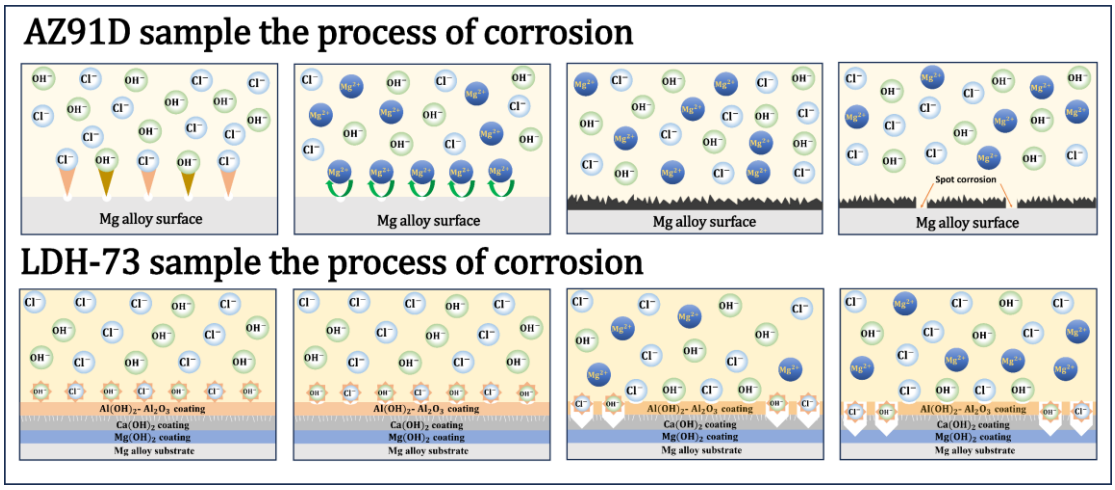


Figure 9. Corrosion of the AZ91D sample and LDH-73 in 3.5 wt% NaCl solution.

4. Summary

A LDH-73 composite coating with outstanding corrosion resistance was fabricated on the surface of Mg substrates via the hydrothermal method. The coating primarily consists of $Mg(OH)_2$, $Ga(OH)_2$, $Al(OH)_3$, and Al_2O_3, where $Ga(OH)_2$, $Al(OH)_3$, and Al_2O_3 fill and reinforce cracks in the $Mg(OH)_2$ coatings. The formation mechanism of the coating was analyzed in this study. Electrochemical tests indicated the coating possessed excellent corrosion resistance, with impedance values four orders of magnitude higher and corrosion current density reduced by three orders compared to the bare magnesium substrate. Additionally, immersion in 3.5% NaCl solution confirmed the coating's good long-term corrosion resistance and durability. The cross-cut tape test further demonstrated the coating's good adhesion performance. Compared to existing coatings, this coating preparation process is green, pollution-free, and uses readily available reagents. It not only ensures good corrosion resistance but also exhibits excellent environmental and biocompatibility properties. Additionally, its application in the medical device and automotive manufacturing industries shows great potential, extending the lifespan of medical devices and protecting metal components from corrosion. To optimize the coating's performance, further investigation into its long-term stability and durability in various corrosive environments will be conducted. In summary, the coating prepared by this method offers convenience, simplicity, and effectiveness. The composite coating provides a new approach to protect magnesium alloys, widening application and extending life.

Author Contributions: Methodology, J.Z.; Validation, Q.T.; Formal analysis, Y.Z.; Investigation, Y.Z., M.J. and J.Z.; Writing—original draft, Q.T. All authors have read and agreed to the published version of the manuscript.

Funding: The author thanks the Natural Science Foundation of Guangxi (Grant 2023GXNSFAA026371) for supported.

Institutional Review Board Statement: Not applicable.

Informed Consent Statement: Not applicable.

Data Availability Statement: Data are contained within the article.

Conflicts of Interest: The authors declare no conflicts of interest.

References

1. Aydin, F. Recent advances in mechanical properties of Mg matrix composites: A review. *Mater. Sci. Technol.* **2024**, *40*, 339–376. [CrossRef]
2. Zhang, Z.M.; Yu, J.M.; Xue, Y.; Dong, B.B.; Zhao, X.; Wang, Q. Recent research and development on forming for large magnesium alloy components with high mechanical properties. *J. Magnes. Alloys* **2023**, *11*, 4054–4081. [CrossRef]
3. Yang, H.; Xie, W.L.; Song, J.F.; Dong, Z.H.; Gao, Y.Y.; Jiang, B.; Pan, F.S. Current progress of research on heat-resistant Mg alloys: A review. *Int. J. Miner. Metall. Mater.* **2024**, *31*, 1406–1425. [CrossRef]
4. Zhang, G.Q.; Zhang, S.S.; Song, R.B.; Cai, C.H. Effect of Mg and Si contents on hot-dip 55Al-Zn plating: Experimental and molecular dynamics simulation. *Mater. Today Commun.* **2023**, *35*, 106131. [CrossRef]
5. Kim, S.H.; Jo, H.J.; Lee, S.H.; Lee, M.H. Unique Anti-Corrosion Performance of Al-Mg-Si Film on Steel Plate Formed by Heat Treatment. *Sci. Adv. Mater.* **2022**, *14*, 1204–1212. [CrossRef]
6. Moussa, M.E.; El-Hadad, S.; Nofal, A. Influence of Si Addition on the Microstructure, Hardness and Elevated-Temperature Sliding Wear Behavior of AX53 Magnesium Alloy. *Int. J. Met.* **2022**, *16*, 385–398. [CrossRef]
7. Calderón, H.E.; Hidalgo, R.G.I.; Melgarejo, Z.H.; Suárez, O.M. Effect of AlB2-Mg interaction on the mechanical properties of Al-based composites. *Mater. Sci. Eng. A Struct. Mater. Prop. Microstruct. Process.* **2010**, *527*, 2258–2264. [CrossRef]
8. Ueda, T.; Nagao, M.; Ikeo, N.; Washio, K.; Kinoshita, A.; Kato, A.; Mukai, T. Impact Energy Absorption Capability of Magnesium Alloy Pipe. *J. Jpn. Inst. Met. Mater.* **2014**, *78*, 142–148. [CrossRef]
9. Liu, L.Z.; Chen, X.H.; Pan, F.S. A review on electromagnetic shielding magnesium alloys. *J. Magnes. Alloys* **2021**, *9*, 1906–1921. [CrossRef]
10. Luo, Z.; Chen, X.H.; Song, K.; Liu, C.Q.; Dai, Y.; Zhao, D.; Pan, F.S. Effect of Alloying Element on Electromagnetic Interference Shielding Effectiveness of Binary Magnesium Alloys. *Acta Metall. Sin.-Engl. Lett.* **2019**, *32*, 817–824. [CrossRef]
11. Murugesan, R.; Venkataramana, S.H.; Marimuthu, S.; Anand, P.B.; Nagaraja, S.; Isaac, J.S.; Sudharsan, R.R.; Khan, T.M.Y.; Almakayeel, N.; Islam, S.; et al. Influence of Alloying Materials Al, Cu, and Ca on Microstructures, Mechanical Properties, And Corrosion Resistance of Mg Alloys for Industrial Applications: A Review. *ACS Omega* **2023**, *8*, 37641–37653. [CrossRef] [PubMed]
12. You, F.F.; Liu, X.Y.; Ying, M.W.; Yang, Y.J.; Ke, Y.T.; Shen, Y.; Tong, G.X.; Wu, W.H. In situ generated gas bubble-directed self-assembly of multifunctional MgO-based hybrid foams for highly efficient thermal conduction, microwave absorption, and self-cleaning. *Mater. Horiz.* **2023**, *10*, 4609–4625. [CrossRef] [PubMed]
13. Wei, C.L.; Tan, L.W.; Zhang, Y.C.; Wang, Z.R.; Feng, J.K.; Qian, Y.T. Towards better Mg metal anodes in rechargeable Mg batteries: Challenges, strategies, and perspectives. *Energy Stor. Mater.* **2022**, *52*, 299–319. [CrossRef]
14. Gong, B.S.; Huang, Q.; Xia, G.H.; Habibullah; Wu, J.A.; Guo, C.; Wang, Y.; Yan, Y.G.; Chen, Y.G.; Wu, C.L. Challenges and breakthroughs of Mg-based materials for hydrogen generation by hydrolysis. *Int. J. Hydrogen Energy* **2025**, *105*, 1008–1025. [CrossRef]
15. Costa, V.; Raimondi, L.; Scilabra, S.D.; Lo Pinto, M.; Bellavia, D.; De Luca, A.; Guglielmi, P.; Cusanno, A.; Cattini, L.; Pulsatelli, L.; et al. Effect of Hydrothermal Coatings of Magnesium AZ31 Alloy on Osteogenic Differentiation of hMSCs: From Gene to Protein Analysis. *Materials* **2025**, *18*, 1254. [CrossRef]
16. Han, Q.; Zhang, X.P.; Li, W.; Tian, A.X.; Ma, X.L.; Zhao, Y.; Chen, M.F. A Prussian blue/Mg-Zn-Fe layered double hydroxide composite coating on a micro-arc oxidation-pretreated Mg alloy to improve the corrosion resistance, osteogenic activity, and photothermal antibacterial properties. *Mater. Today Commun.* **2025**, *45*, 112263. [CrossRef]
17. Nagaraja, S.; Anand, P.B.; Mariswamy, M.; Alkahtani, M.Q.; Islam, S.; Khan, M.A.; Khan, W.A.; Bhutto, J.K. Friction stir welding of dissimilar Al-Mg alloys for aerospace applications: Prospects and future potential. *Rev. Adv. Mater. Sci.* **2024**, *63*, 20240033. [CrossRef]
18. Tekumalla, S.; Gupta, M. An insight into ignition factors and mechanisms of magnesium based materials: A review. *Mater. Des.* **2017**, *113*, 84–98. [CrossRef]
19. Oishi, M.; Ichitsubo, T.; Okamoto, S.; Toyoda, S.; Matsubara, E.; Nohira, T.; Hagiwara, R. Electrochemical Behavior of Magnesium Alloys in Alkali Metal-TFSA Ionic Liquid for Magnesium-Battery Negative Electrode. *J. Electrochem. Soc.* **2014**, *161*, A943–A947. [CrossRef]
20. Lv, Y.Z.; Liu, M.; Xu, Y.; Cao, D.X.; Feng, J.; Wu, R.Z.; Zhang, M.L. The electrochemical behaviors of Mg-8Li-0.5Y and Mg-8Li-1Y alloys in sodium chloride solution. *J. Power Sourc.* **2013**, *239*, 265–268. [CrossRef]
21. Ouyang, Y.B.; Guo, E.Y.; Chen, X.B.; Kang, H.J.; Chen, Z.N.; Wang, T.M. Recent progress in protective coatings against corrosion upon magnesium-lithium alloys: A critical review. *J. Magnes. Alloys* **2024**, *12*, 3967–3995. [CrossRef]
22. Esmaily, M.; Svensson, J.E.; Fajardo, S.; Birbilis, N.; Frankel, G.S.; Virtanen, S.; Arrabal, R.; Thomas, S.; Johansson, L.G. Fundamentals and advances in magnesium alloy corrosion. *Prog. Mater. Sci.* **2017**, *89*, 92–193. [CrossRef]
23. Hsiao, W.L.; Chu, P.W. Fabrication of Vanadate-Exchanged Electrodeposited Zn-Al Layered Double Hydroxide (LDH) Coating on a ZX21 Mg Alloy to Improve the Corrosion Resistance. *Coatings* **2024**, *14*, 1047. [CrossRef]

24. Han, X.; Wang, Y.; Ma, J.X.; Ma, X.L. Corrosion Resistance and In Vitro Biological Properties of TiO_2 on MAO-Coated AZ31 Magnesium Alloy via ALD. *Coatings* **2024**, *14*, 1198. [CrossRef]
25. Di Egidio, G.; Tonelli, L.; Morri, A.; Boromei, I.; Shashkov, P.; Martini, C. Influence of Anodizing by Electro-Chemical Oxidation on Fatigue and Wear Resistance of the EV31A-T6 Cast Magnesium Alloy. *Coatings* **2023**, *13*, 62. [CrossRef]
26. Li, L.Y.; Cui, L.Y.; Liu, B.; Zeng, R.C.; Chen, X.B.; Li, S.Q.; Wang, Z.L.; Han, E.H. Corrosion resistance of glucose-induced hydrothermal calcium phosphate coating on pure magnesium. *Appl. Surf. Sci.* **2019**, *465*, 1066–1077. [CrossRef]
27. Kotoka, R.; Yamoah, N.K.; Mensah-Darkwa, K.; Moses, T.; Kumar, D. Electrochemical corrosion behavior of silver doped tricalcium phosphate coatings on magnesium for biomedical application. *Surf. Coat. Technol.* **2016**, *292*, 99–109. [CrossRef]
28. Xie, J.S.; Zhang, J.H.; Liu, S.J.; Li, Z.H.; Zhang, L.; Wu, R.Z.; Hou, L.G.; Zhang, M.L. Hydrothermal Synthesis of Protective Coating on Mg Alloy for Degradable Implant Applications. *Coatings* **2019**, *9*, 160. [CrossRef]
29. Wang, X.G.; Yan, L.C.; Gao, K.W.; Li, P.C.; Hao, J.J. Enhancing the Corrosion Resistance of ZnAl-LDHs Films on AZ91D Magnesium Alloys by Designing Surface Roughness. *Coatings* **2023**, *13*, 724. [CrossRef]
30. Yigit, O.; Gurgenc, T.; Dikici, B.; Kaseem, M.; Boehlert, C.; Arslan, E. Surface Modification of Pure Mg for Enhanced Biocompatibility and Controlled Biodegradation: A Study on Graphene Oxide (GO)/Strontium Apatite (SrAp) Biocomposite Coatings. *Coatings* **2023**, *13*, 890. [CrossRef]
31. Khan, M.A.; Safira, A.R.; Aadil, M.; Kaseem, M. Development of anti-corrosive coating on AZ31 Mg alloy modified by MOF/LDH/PEO hybrids. *J. Magnes. Alloys* **2024**, *12*, 586–607. [CrossRef]
32. Zhang, J.M.; Lian, D.D.; Hou, A.R.; Wang, Z.H.; Zhang, M.C.; Wu, J.W.; Wang, C.C. Comparative Study on Microstructure, Corrosion Morphology, and Friction Wear Properties of Layered Double Hydroxide/Steam Coating Composite Coatings on Mg-Li Alloy. *Adv. Eng. Mater.* **2024**, *26*, 2400058. [CrossRef]
33. Liu, L.; Lei, J.L.; Li, L.J.; Zhang, X.P.; Li, N.B.; Pan, F.S. Constructing Colorful Surfaces with Mechanical Robustness for Magnesium Alloys via a Reagent-Free Method. *ACS Appl. Mater. Interfaces* **2020**, *12*, 48206–48215. [CrossRef] [PubMed]
34. Zhu, J.Y.; Jia, C.X.; Duan, Y.Z. Study on Corrosion Resistance of Alkali-Heat Modified Magnesium Alloy Surface. *Met. Mater. Int.* **2023**, *29*, 1638–1651. [CrossRef]
35. Yao, Z.H.; Wang, D.J.; Xu, N.; Du, C.S.; Feng, Y.F.; Qi, Y.J. Phosphate and humic acid inhibit corrosion of green-synthesized nano-iron particles to remove Cr(VI) and facilitate their cotransport. *Chem. Eng. J.* **2022**, *450*, 136415. [CrossRef]
36. Amala, A.; Franco, P.A.; Binoj, J.S.; Shemin, A.A. Mechanical, morphological and water intake behavior of Mg-Si integrated carbon hybrid composite for marine deckhouse. *Rev. Metal.* **2023**, *59*, e246. [CrossRef]
37. Wang, Y.; Xiao, W.X.; Ma, K.; Dai, C.E.; Wang, D.Q.; Wang, J.F.; Pan, F.S. Towards development of anticorrosive $CaCO_3$-coated passive layer on Mg alloy with ultrasound-assisted electrodeposition. *Corros. Sci.* **2023**, *224*, 111546. [CrossRef]
38. Hou, R.Q.; Li, Y.Q.; Jiang, P.L.; Zhu, S.J.; Wang, L.G.; Guan, S.K. The regulation of organic molecules to the morphology and corrosion protection ability of $CaCO_3$ coating on biomedical MgZnCa alloy. *Surf. Coat. Technol.* **2024**, *478*, 130425. [CrossRef]
39. Zhang, J.M.; Li, J.C.; Hou, A.R.; Lian, D.D.; Zhang, M.C.; Wang, Z.H.; Zhang, T. A comparative study and optimization of corrosion resistance of Mg-Al layered double hydroxides films at different hydrothermal temperatures on LA103Z Mg-Li alloy. *Mater. Corros.* **2023**, *74*, 597–607. [CrossRef]
40. *ASTM G31-72(2004)*; Standard Practice for Laboratory Immersion Corrosion Testing of Metals. ASTM International: West Conshohocken, PA, USA, 2004.
41. Suchanek, W.L. Hydrothermal Synthesis of Alpha Alumina (α-Al_2O_3) Powders: Study of the Processing Variables and Growth Mechanisms. *J. Am. Ceram. Soc.* **2010**, *93*, 399–412. [CrossRef]
42. Zhao, Y.; Tian, A.X.; Wang, W.; Chen, Y.P.; Li, W.; Liu, W.; Chen, M.F. The Effects of Reaction Parameters on the Corrosion Resistance of an Mg-Al Hydroxide Coating via in Situ Growth on a Biomedical Magnesium Alloy. *Coatings* **2022**, *12*, 1388. [CrossRef]
43. Li, Q.Y.; Lu, H.; Cui, J.; An, M.Z.; Li, D.Y. Understanding the low corrosion potential and high corrosion resistance of nano-zinc electrodeposit based on electron work function and interfacial potential difference. *RSC Adv.* **2016**, *6*, 97606–97612. [CrossRef]
44. Heakal, F.E.T.; Fekry, A.M.; Fatayerji, M.Z. Influence of halides on the dissolution and passivation behavior of AZ91D magnesium alloy in aqueous solutions. *Electrochim. Acta* **2009**, *54*, 1545–1557. [CrossRef]
45. Hoche, H.; Schmidt, J.; Gross, S.; Trossmann, T.; Berger, C. PVD coating and substrate pretreatment concepts for corrosion and wear protection of magnesium alloys. *Surf. Coat. Technol.* **2011**, *205*, S145–S150. [CrossRef]
46. Huang, L.N.; Luo, Q.; He, Y. Assessment of Corrosion Protection Performance of FeOOH/Fe_3O_4/C Composite Coatings Formed In Situ on the Surface of Fe Metal in Air-Saturated 3.5 wt.% NaCl Solution. *Materials* **2023**, *16*, 224. [CrossRef]
47. Fischer, D.A.; Vargas, I.T.; Pizarro, G.E.; Armijo, F.; Walczak, M. The effect of scan rate on the precision of determining corrosion current by Tafel extrapolation: A numerical study on the example of pure Cu in chloride containing medium. *Electrochim. Acta* **2019**, *313*, 457–467. [CrossRef]
48. *ASTM-D3359-23*; Standard Test Methods for Rating Adhesion by Tape Test. ASTM International: West Conshohocken, PA, USA, 2023.

49. *ISO 2409:2020*; Paints and Varnishes—Cross-Cut Test. ISO: Geneva, Switzerland, 2020.
50. Wang, Y.C.; Liu, B.Y.; Zhao, X.A.; Zhang, X.H.; Miao, Y.C.; Yang, N.; Yang, B.; Zhang, L.Q.; Kuang, W.J.; Li, J.; et al. Turning a native or corroded Mg alloy surface into an anti-corrosion coating in excited CO_2. *Nat. Commun.* **2018**, *9*, 4058. [CrossRef]
51. Zhu, Y.Y.; Zhao, Q.; Zhang, Y.H.; Wu, G.M. Hydrothermal synthesis of protective coating on magnesium alloy using de-ionized water. *Surf. Coat. Technol.* **2012**, *206*, 2961–2966. [CrossRef]

Disclaimer/Publisher's Note: The statements, opinions and data contained in all publications are solely those of the individual author(s) and contributor(s) and not of MDPI and/or the editor(s). MDPI and/or the editor(s) disclaim responsibility for any injury to people or property resulting from any ideas, methods, instructions or products referred to in the content.